

Elastic properties of a tungsten-silver composite by reconstruction and computation*

A. P. Roberts[†]

University of Oxford, Department of Materials,
Parks Rd, Oxford OX1-3PH, U.K.

and

E. J. Garboczi

Building Materials Division,
National Institute of Standards and Technology,
100 Bureau Drive Stop 8621, Gaithersburg, MD 20899-8621, U.S.A.

March 26, 2021

Keywords: structure-property relationships; microstructures (A); inhomogeneous material (B); finite elements (C); probability and statistics (C).

Abstract

We statistically reconstruct a three-dimensional model of a tungsten-silver composite from an experimental two-dimensional image. The effective Young's modulus (E) of the model is computed in the temperature range 25–1060°C using a finite element method. The results are in good agreement with experimental data. As a test case, we have reconstructed the microstructure and computed the moduli of the overlapping sphere model. The reconstructed and overlapping sphere models are examples of bi-continuous (non-particulate) media. The computed moduli of the models are not generally in good agreement with the predictions of the self-consistent method. We have also evaluated three-point variational bounds on the Young's moduli of the models using the results of Beran, Molyneux, Milton and Phan-Thien. The measured data were close to the upper bound if the properties of the two phases were similar ($\frac{1}{6} < E_1/E_2 < 6$).

1 Introduction

Predicting the macroscopic properties of composite or porous materials with random microstructures is an important problem in a range of fields [6, 19, 41, 38]. There now exist large-scale computational methods for calculating the properties of composites given a digital representation of their microstructure; eg. permeability [4, 2], conductivity [3, 37] and elastic moduli [18, 29]. A critical problem is obtaining an accurate three-dimensional (3D) description of this microstructure [4, 15, 48].

For particular materials it may be possible to simulate microstructure formation from first principles. Generally this relies on detailed knowledge of the physics and chemistry of the system, with accurate modeling of each material requiring a significant amount of research.

*Submitted to J. Mech. Phys. Solids

[†]Permanent address: Centre for microscopy and microanalysis, University of Queensland, Brisbane, Queensland 4072, Australia

Three-dimensional models have also been directly reconstructed from samples by combining digitized serial sections obtained by scanning electron microscopy [26], or using the relatively new technique of x-ray microtomography [16]. In the absence of sophisticated experimental facilities, or a sufficiently detailed description of the microstructure formation (for computer simulation), a third alternative is to employ a statistical model of the microstructure. This procedure has been termed “statistical reconstruction” since the statistical properties of the model are matched to those of a two-dimensional (2D) image [30, 3, 4, 34]. Statistical reconstruction is a promising method of producing 3D models, but there remain outstanding theoretical questions regarding its application. First, what is the most appropriate statistical information (in a 2D image) for reconstructing a 3D image, and second, is this information sufficient to produce a useful model? In this paper we address these questions, and test the method against experimental data.

Modeling a composite and numerically estimating its macroscopic properties is a complex procedure. This could be avoided if accurate analytical structure-property relations could be theoretically or empirically obtained. Many studies have focussed on this problem [19]. In general, the results are reasonable for a particular class of composites or porous media. The self-consistent (or effective medium) method of Hill [22] and Budiansky [11] and its generalization by Christensen and Lo [13] is one of the most common for particulate media [19]. No analogous results are available for non-particulate composites. A promising alternative to direct property prediction has been the development of analytical rigorous bounds (reviewed by Willis [47], Hashin [19] and Torquato [41]). There is a whole hierarchy of these bounds, each set tighter than the next, but depending on higher and higher order correlation functions of the microstructure. The original Hashin and Shtrikman [20] bounds that have been widely used by experimentalists implicitly depend on the two-point correlation function of the microstructure, although the only quantities appearing in the formulas are the individual properties of each phase and their volume fractions. To go beyond these bounds to higher-order, more restrictive (i.e., narrower) bounds, it is necessary that detailed information be known about the composite in the form of three-point or higher statistical correlation functions [5, 28], which do appear explicitly in the relevant formulas. Evaluation of even the three point function is a formidable task, so use of these bounds has in the past been restricted to composites with spherical inclusions. It is now possible to evaluate the bounds for non-particulate composites [37], and it is interesting to compare the results with experimental and numerical data. If the properties of each phase are not too dissimilar the bounds are quite restrictive and can be used for predictive purposes [20]. Sometimes experimental properties closely follow one or the other of the bounds, so that the upper or lower bound often provides a reasonable prediction of the actual property even when the phases have very different properties [41, 35]. It is useful to test this observation.

In this study we test a generalized version [34] of Quiblier’s [30] statistical reconstruction procedure on a well-characterized silver-tungsten composite. Computational estimates of the Young’s moduli are compared to experimental measurements. The composite is bi-continuous (both phases are macroscopically connected) and therefore has a non-particulate character. As such the microstructure is broadly representative of that observed in open-cell foams (such as aerogels), polymer blends, porous rocks, and cement-based materials. By comparing our computations of the moduli to the results of the self-consistent method we can test its utility for non-particulate media. An advantage of the reconstruction procedure we use is that it provides the statistical correlation functions necessary for evaluating the three-point bounds. Comparison of the Young’s modulus to the bounds therefore allows us to determine the bounds’ range of application for predictive purposes.

2 Statistical models of microstructure

The two basic models we employ to describe two-phase composite microstructure are the overlapping sphere model and the level-cut Gaussian random field (GRF) model. In this section we review the statistical properties of these models which are useful for reconstructing composites. The simplest, and most common, quantities used to characterize random microstructure are p , the volume fraction of phase 1, s_v , the surface area to total volume ratio and $p^{(2)}(r)$, the two-point correlation function (or $\gamma(r) \equiv [p^{(2)}(r) - p^2]/[p - p^2]$ the auto-correlation function). $p^{(2)}(r)$ represents the probability that two points a distance r apart lie in phase 1. Here we only consider isotropic materials where $p^{(2)}$ does not depend on direction. Also note that $p = p^{(2)}(0)$ and $s_v = -4dp^{(2)}(0)/dr$.

Realizations of the overlapping sphere model [46] are generated by randomly placing spheres (of radii r_0) into a matrix. The correlation function of the phase exterior to the spheres (fraction p) is $p^{(2)}(r) = p^{v(r)}$ for $r < 2r_0$ and $p^{(2)}(r) = p^2$ for $r \geq 2r_0$ where

$$v(r) = 1 + \frac{3}{4} \left(\frac{r}{r_0} \right) - \frac{1}{16} \left(\frac{r}{r_0} \right)^3, \quad (1)$$

and the surface to volume ratio is $s_v = -3p \ln p / r_0$. With modification it is also possible to incorporate poly-dispersed and/or hollow spheres. The overlapping sphere model is the most well characterized of a wider class called Boolean models, which have been recently reviewed by Stoyan *et al.* [39].

The internal interfaces of a different class of composites can be modeled by the iso-surfaces (or level-cuts) of a stationary correlated Gaussian random field (GRF) $y(\mathbf{r})$ (so called because the value of the field at randomly chosen points in space is Gaussian-distributed). Moreover, if \mathbf{r} is fixed, the distribution over an ensemble will also be Gaussian. Correlations in the field are governed by the field-field correlation function $g(r) = \langle y(0)y(\mathbf{r}) \rangle$ which can be specified subject to certain constraints [$|g(r)| < g(0)$, $\lim_{r \rightarrow \infty} g(r) \rightarrow 0$]. Invariably $g(0)$ is taken as unity. A useful general form for g is [34]

$$g(r) = \frac{e^{-r/\xi} - (r_c/\xi)e^{-r/r_c} \sin 2\pi r/d}{1 - (r_c/\xi)} \frac{\sin 2\pi r/d}{2\pi r/d}. \quad (2)$$

The resulting field is characterized by a correlation length ξ , domain scale d and a cut-off scale r_c . The cut-off scale is necessary to ensure $1 - g(r) \sim r^2$ as $r \rightarrow 0$; fractal iso-surfaces are generated if $1 - g(r) \sim r$. There are many algorithmic methods of generating random fields. A straight forward method is to sum N (~ 1000) sinusoids with random phase and wave-vector

$$y(\mathbf{r}) = \sqrt{\frac{2}{N}} \sum_{i=1}^N \cos(k_i \hat{\mathbf{k}}_i \cdot \mathbf{r} + \phi_i), \quad (3)$$

where ϕ_i is a uniform deviate on $[0, 2\pi)$ and $\hat{\mathbf{k}}_i$ is uniformly distributed on a unit sphere. The magnitude of the wave vectors k_i are distributed on $[0, \infty)$ with a probability (spectral) density $P(k)$. The density is related to $g(r)$ by a Fourier transform [$g(r) = \int_0^\infty P(k) \sin kr (kr)^{-1} dk$]. Note that $P(k) > 0$ specifies an additional constraint on $g(r)$. Although this formulation of a GRF is intuitive, the Fast Fourier Transform method is more efficient [1, 37].

Following Berk [7] one can define a composite with phase 1 occupying the region in space where $\alpha \leq y(\mathbf{r}) \leq \beta$ and phase 2 occupying the remainder. The statistics of the material are completely determined by the specification of the level-cut parameters and the function $g(r)$ (or $P(k)$). The volume fraction of phase 1 is

$$p = h = p_\beta - p_\alpha \quad \text{where} \quad p_\gamma = (2\pi)^{-\frac{1}{2}} \int_{-\infty}^{\gamma} e^{-t^2/2} dt, \quad \gamma = \alpha, \beta. \quad (4)$$

Table 1: The volume fraction p , two-point correlation function $p_2(r)$ and surface to volume ratio s_v of models N, I, U and I_n in terms of the properties $[h, h(r)$ and $h'(0)]$ of Berk's two-level cut Gaussian random field model. The formula h_p is used for calculating the level-cut parameters (see Table 2).

Mod.	p	$p^{(2)}(r)$	s_v	h_p
N	h	$h(r)$	$-4h'(0)$	p
I	h^2	$h^2(r)$	$-8hh'(0)$	\sqrt{p}
U	$h(2-h)$	$[2h^2 + 2h(r) - 4hh(r) + h^2(r)]$	$-8(1-h)h'(0)$	$1 - \sqrt{1-p}$
I_n	h^n	$h^n(r)$	$-4nh^{n-1}h'(0)$	$p^{1/n}$

Berk [7] and Teubner [40] have shown that the two point correlation function is $p^{(2)}(r) = h(r)$ where

$$h(r) = h^2 + \frac{1}{2\pi} \int_0^{g(r)} \frac{dt}{\sqrt{1-t^2}} \times \left[\exp\left(-\frac{\alpha^2}{1+t}\right) - 2 \exp\left(-\frac{\alpha^2 - 2\alpha\beta t + \beta^2}{2(1-t^2)}\right) + \exp\left(-\frac{\beta^2}{1+t}\right) \right]. \quad (5)$$

The auxiliary variables h and $h(r)$ are needed below. The singularity at $t = 1$ can be removed with the substitution $t = \sin \theta$. The specific surface is $s_v = -4h'(0)$ where

$$-h'(0) = \frac{\sqrt{2}}{2\pi} \left(e^{-\frac{1}{2}\alpha^2} + e^{-\frac{1}{2}\beta^2} \right) \sqrt{\frac{4\pi^2}{6d^2} + \frac{1}{2r_c\xi}} \quad (6)$$

with g given by Eqn. (2).

Many more models (for which $p^{(2)}(r)$ can be simply evaluated) can be formed from the intersection and union sets of the overlapping sphere and level-cut GRF models. Here we define a few representative models which have been shown to be applicable to composite and porous media. A normal model (N) corresponds to Berk's formulation. Models can also be formed from the intersection (I) and union (U) of two statistically identical level-cut GRF's. Another model, I_n , formed from the intersection of n primary models, has also been found useful. The statistical properties (p , s_v and $p^{(2)}$) of each model are given in terms of the properties of Berk's model [Eqns. (4), (5) and (6)] in Table 1 [34].

Since the volume fraction of the models is a function of both level-cut parameters (α, β) there is a continuum of choices which correspond to a given volume fraction. For example $(\alpha, \beta) = (-\infty, 0.84)$, $(-0.84, -0.25)$, $(-0.25, 0.25)$, $(0.25, 0.84)$ and $(0.84, \infty)$ in Berk's model all correspond to $p = 20\%$. The final two choices are statistically identical to the first two and therefore provide nothing new. We note that a small change in these parameters will only slightly alter the microstructure, so as a compromise between simplicity and generality it is suggested only three distinct cases be considered: (i) the common single-cut field ($\alpha = -\infty$); (ii) a symmetric two-cut field ($\alpha = -\beta$) and (iii) an asymmetric two-cut field. A concise way of expressing this is to take $p_\alpha = \frac{c}{2} - \frac{c}{2}h_p$ and $p_\beta = \frac{c}{2} + (1 - \frac{c}{2})h_p$ where h_p for models N, I, U and I_n is given in Table 1 and $c \in [0, 1]$. Setting $c=0$, 1 and $\frac{1}{2}$ gives cases (i), (ii) and (iii) respectively. The implicit formula for finding (α, β) from p_α and p_β is shown in Eqn. (4). As an example the results of the calculation for nine different models (N, I and U at $c=0$, $\frac{1}{2}$ and 1) at volume fraction 20% is shown in Table 2. The model N ($c=0$) is the single level

Table 2: The level-cut parameters α and β for different Gaussian random field models are calculated by solving Eqn. (4) where $p_\alpha = \frac{c}{2} - \frac{c}{2}h_p$ and $p_\beta = \frac{c}{2} + (1 - \frac{c}{2})h_p$. h_p is shown in Table 1 for each model and $c = 0, \frac{1}{2}, 1$. This table shows the results of the calculation for volume fraction $p=20\%$.

Model type	Standard one-cut		Asymmetric two-cut		Symmetric two-cut	
	$c = 0$		$c = 1/2$		$c = 1$	
	α	β	α	β	α	β
Normal (N)	$-\infty$	-0.84	-0.84	-0.25	-0.25	0.25
Intersection (I)	$-\infty$	-0.13	-1.09	0.22	-0.59	0.59
Union (U)	$-\infty$	-1.25	-0.76	-0.44	-0.13	0.13

cut GRF previously used by Quiblier [30] and Teubner [40]. Model I ($c=1$) has been used to model aerogels [33] and model N ($c=1$) is Berk's [7] two level cut model of microemulsions.

3 Statistical reconstruction

3.1 The Joshi-Quiblier-Adler (JQA) Approach

The basic idea of statistical reconstruction is to generate a three dimensional (3D) model of a random composite using only statistical information measured from a two dimensional (2D) image. Since 2D cross-sections are readily obtained by common experimental methods this provides a very attractive method of modeling porous and composite media. Quiblier [30] developed a method capable of producing a three-dimensional model with a specified volume fraction and two-point correlation function. The method was first studied in two dimensions by Joshi [24] and has been extended by Adler [1]. Thus it has been called the JQA model. We first give a summary of the procedure to demonstrate its equivalence to the single-cut GRF model discussed in the last section. First p and $p_{\text{expt}}^{(2)}$ are measured from an experimental image. The level-cut parameter β is fixed by the volume fraction [Eqn. (4) with $\alpha = -\infty$]. Second $g_{\text{expt}}(r_i)$ is obtained at the set of discrete points where $p_{\text{expt}}^{(2)}$ is measured by inverting Eqn. (5) with the left hand side set to $p_{\text{expt}}^{(2)}(r_i)$ and $\alpha = -\infty$. To carry out the inversion the right hand side of Eqn. (5) is expanded as a series in powers of g ;

$$p_{\text{expt}}^{(2)}(r_i) = p^2 + p(1 - p) \sum_{m=0}^{\infty} C_m^2 [g_{\text{expt}}(r_i)]^m \quad (7)$$

where the coefficients C_m depend on certain integrals of Hermite polynomials [30]. The series converges very slowly for g near one, and Alder [1] has discussed the inversion procedure in this case, and possible situations where the equation has no solution. We note that the inversion can also be simply carried out by numerical integration of Eqn. (5) and a standard non-linear equation solver.

Next it is necessary to generate a GRF with field-field correlation function $g_{\text{expt}}(r)$. Quiblier's original formulation involved the solution of a very large system of non-linear equations for the terms of a convolution operator used in his definition of a GRF. Adler [1] simplified the procedure by reformulating the problem in terms of Fourier transforms, which is equivalent to a three-dimensional version [37] of Rice's [32] method for Gaussian processes in one dimension. In terms of the definition given in Eqn. (3) the inversion is equivalent to a

numerical integration of $P(k) = \frac{2}{\pi} \int_0^\infty g(r)rk \sin kr dr$, where g is known only at a discrete set of points. The inversion methods described above for $g(r)$ do not guarantee that $P(k)$ (or its equivalent in other formulations) is greater than zero. However Adler [1] found that if $P(k)$ is negative at some points it is also small, and can be replaced with zero. Finally the GRF is thresholded in the usual way to obtain the reconstructed microstructure. Thus the JQA method produces a single-cut Gaussian random field, which we have termed model N($c=0$).

In this paper we employ a different implementation of the JQA method [34]. At this stage we restrict attention to model N($c=0$). First, the volume fraction of the model is set to that of an image: $p_{\text{mod}}=p_{\text{expt}}$. Second, the experimental two point correlation function is fitted by varying the morphological parameters of a *given* $g(r)$ [Eqn. (2)] to minimize the non-linear least squares error

$$[Ep^{(2)}]^2 = \frac{\sum_{i=1}^{N_f} [p_{\text{mod}}^{(2)}(r_i) - p_{\text{expt}}^{(2)}(r_i)]^2}{\sum_{i=1}^{N_f} [p_{\text{expt}}^{(2)}(r_i) - p_{\text{expt}}^2]^2}. \quad (8)$$

where N_f is the number of experimental points to be fitted. Numerical integration is used to find $p_{\text{mod}}^{(2)}(r_i)$ [Eqn. (5)]. The minimization is very fast, but several starting points should be used as a check against local minima. Once the parameters of $g(r)$ are known an analytic form of $P(k)$ is used to generate the coefficients of the GRF (3). The reconstructed model is obtained by thresholding the random field as described above. Note that $p_{\text{mod}}^{(2)}(r_i)$ will not match $p_{\text{expt}}^{(2)}(r_i)$ exactly at each point as would be the case with Quiblier's procedure. However with this choice of $g(r)$, $P(k)$ is guaranteed to be positive. More general functional forms of $g(r)$ can also be employed.

For isotropic materials p and $p^{(2)}(r)$ can be exactly measured from a two (or one) dimensional image. Hence the application of the JQA method results in a model which shares p , s_v and $p^{(2)}(r)$ with a real composite. The question is whether or not the model provides an accurate and useful representation of the original microstructure. In certain cases it appears to, in other it does not. First, predictions of transport properties (conductivity and permeability) obtained from reconstructed porous models under-estimate experimental and numerical data. Second, the percolation threshold (the volume fraction at which the pore space or inclusion phase is no longer macroscopically connected) of model N($c=0$) is around 10% [37] for the model, but many materials exhibit lower thresholds [36]. Both points indicate that the pores (or inclusions) of the model are not sufficiently well connected to mimic many physical materials. Third, we can test the model by trying to reconstruct several of the distinct models defined in the previous section. The results are shown in Fig 1. Even though model N($c=0$) is able to reproduce the correlation functions reasonably well, the reconstructions (i) do not in all cases appear to reproduce the original microstructure and (ii) look quite similar to one another. This indicates that irrespective of $g(r)$, and the original image, model N($c=0$) can only generate microstructures that are similar to those shown in the final row of Fig. 1.

Quiblier [30] has suggested that the ability of the method to generate a reasonable model depends on the validity of the hypothesis that: *all the necessary information about the morphology is contained in the auto-correlation function*. Suppose this were true. Then since the JQA method is sufficiently general to re-produce all reasonable two-point correlation functions (see Fig. 1), it must also be able to generate all types of morphology. The discussion above (and Fig. 1) indicates that model N($c=0$) can only produce a limited class of microstructure and therefore that the hypothesis is false. This does not mean that the the method cannot produce useful models, but we argue it will do so only when the original material is approximately contained in the same limited class. If it is not, then a model from a different class needs to be considered. We discuss this issue in the following section.

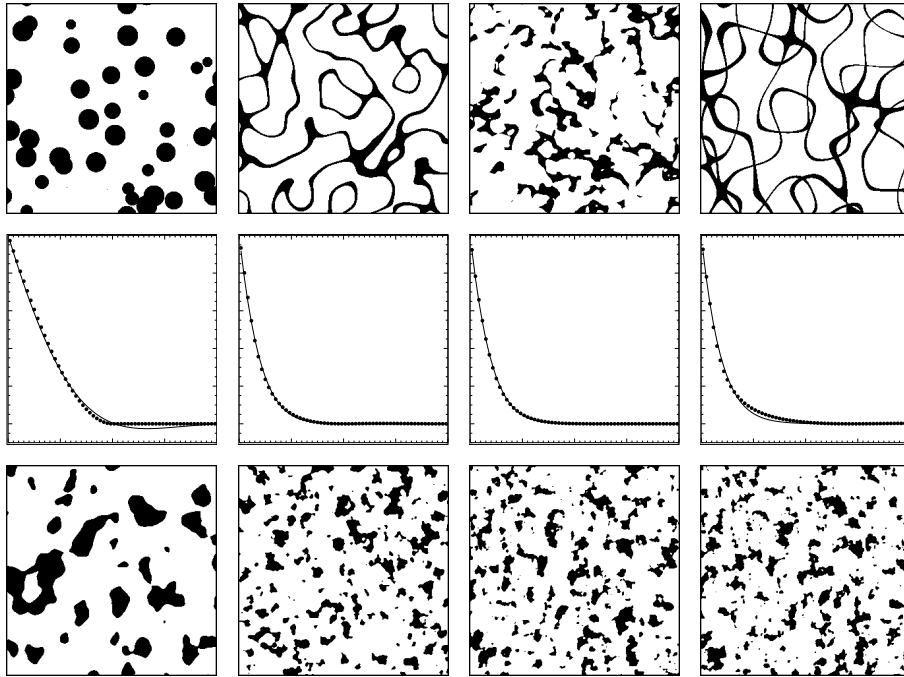


Figure 1: The statistical reconstructions (bottom row) of four different two-dimensional images by adjusting the parameters (r_c , ξ , d and β) of model $N(c=0)$ to fit the auto-correlation functions (middle row) of the original models (shown in the top row). The procedure used is very similar to that of Quiblier. The results suggest that model $N(c=0)$ cannot mimic all types of microstructure, even though it can reproduce the two-point correlation functions of all the cases shown. The models in the top row are (from left to right), overlapping spheres, models $N(c=1)$, $I(c=1)$ and $U(c=1)$ (see Sec. 2). The images are 128×128 pixels, and the length scale of the correlation functions shown in the 2nd row extends to 32 pixels.

3.2 Using several models

From the foregoing discussion it is clear that a model more general than a single level-cut random field is needed to reproduce the random isotropic microstructures seen in many composite materials. At present there is no one model that can achieve this. Instead it has been proposed that a number of morphologically distinct models (N , I and U of Sec. 2) be incorporated [34]. This is very simple to do by using the relevant formula for $p_{\text{mod}}^{(2)}(r)$ (Table 1) in Eqn. (8). It was found that many of these models were able to match any given $p_{\text{expt}}^{(2)}(r)$ (providing further evidence that the two-point correlation function does not provide sufficient information for a useful reconstruction). The problem then becomes how to choose the best model. Clearly higher-order statistical properties need to be taken into account.

The quantities p and $p^{(2)}(r)$ are the first and second of an infinite hierarchy of correlation functions, the three-point function $p^{(3)}(r, s, t)$ representing the probability that three points, distances r , s and t apart fall in phase 1, and so forth. Two random composites can only be said to be statistically identical if their N -th order correlation functions ($N = 1, 2, 3, 4 \dots$) are identical [48]. Therefore the exact statistical reconstruction of a composite requires matching all of the correlation functions¹. An obvious method of choosing the best of several models is then to compare $p^{(3)}$ of each model to experimental data. As well as being memory and time intensive [8] it has been shown [34] that $p^{(3)}$, like $p^{(2)}$, may not contain the relevant

¹Technically, the model and composite may still differ by a point-process [39], but this is unlikely to effect the macroscopic properties.

morphological information (ie. it does not provide a strong signature of microstructure). A comparative study of several high-order statistical quantities found that the simplest and most discriminating signature of microstructure was the chord-distribution functions for each phase $\rho^{(j)}(r)$ ($j = 1, 2$). $\rho^{(j)}(r)$ is the probability that a randomly chosen chord in phase j has length r . A chord is defined as any line-segment which lies entirely in phase j with end points at the phase interface. Like $p^{(2)}$ the chord functions are the same whether measured from a two or three dimensional element of the microstructure.

The chord-functions can be employed in a reconstruction algorithm as follows. First the morphological parameters [the length scales in Eqns. (1) and (2)] of each model (overlapping spheres, or the various level-cut GRF's) are chosen to fit $p_{\text{expt}}^{(2)}$. We have found that most models are able to provide a reasonable fit of $p_{\text{expt}}^{(2)}(r)$ (e.g. $Ep^{(2)} < 0.1$). If this is not the case the model is unlikely to provide a useful reconstruction and may be rejected. Second, of the remaining candidates, the model that best reproduces the experimental chord functions $\rho_{\text{expt}}^{(j)}$ is selected as the best reconstruction. We quantify the error by a normalised least square sum;

$$[E\rho^{(j)}]^2 = \frac{\sum_{i=1}^M [\rho_{\text{rec}}^{(j)}(r_i) - \rho_{\text{expt}}^{(j)}(r_i)]^2}{\sum_{i=1}^M [\rho_{\text{expt}}^{(j)}(r_i)]^2} \quad (9)$$

where $\rho_{\text{rec}}^{(j)}$ are the measured chord-distributions of the reconstruction for phase $j = 1, 2$ (at M points). The final reconstruction thus has approximately the same chord functions as the experimental image as well as sharing the low-order quantities p and $p^{(2)}(r)$.

A limitation of this ‘model-based’ technique is that one of the of models tested must, for some choice of its morphological parameters, be able to approximately reproduce the experimental microstructure. For example, it would be unlikely that a model derived from the iso-surfaces of a random field would be able to mimic the highly structured morphology of randomly packed hard spheres. In such a case we would expect that none of the model chord functions would reproduce the experimental data. At present there have not been a sufficient number of studies to provide numerical criteria on $E\rho^{(j)}$ for acceptability. The general approach we have outlined is not restricted to the models given in Sec. 2. Ultimately it would be useful to incorporate poly-disperse overlapping spheres and other Boolean models such as those based on Poisson and Voronoi polyhedra. The latter models have proved useful in the analysis of mineralogical materials [25] and flow in porous filters [10]. There may also prove to be more useful discriminants of microstructure than the chord-functions.

To conclude this section we note that a recent study [49] has considered a ‘model independent’ scheme based on sequentially moving filled pixels (representing the target phase) on a grid so that the reconstruction reproduces statistical properties of the original image. The method differs from ours in that numerical estimates of $p_{\text{rec}}^{(2)}$ replace $p_{\text{mod}}^{(2)}$ in Eqn. (8), and Eqns. (8) and (9) are coupled. The authors also employ the lineal path distribution function $L^{(j)}(r)$ in Eqn. (9) which is related to the pore-chord functions by $\rho^{(j)}(r) = \frac{1}{4}s_v d^2 L^{(j)}(r)/dr^2$ [43].

4 Elastic properties

4.1 Theory

The basic information required for the evaluation of the effective moduli are the volume fractions, and elastic moduli, of each phase; p (fraction of phase 1), $q = 1 - p$, κ_i and μ_i ($i = 1, 2$). A common approximation for the effective moduli is the self-consistent method (SCM) of Hill [22] and Budiansky [11] which involves solving the equations of elasticity for

a spherical particle of phase 1 surrounded by a medium of unknown effective moduli κ_e, μ_e . The results are obtained by solving

$$\frac{p}{\kappa_e - \kappa_2} + \frac{q}{\kappa_e - \kappa_1} = \frac{3}{3\kappa_e + 4\mu_e} \quad (10)$$

$$\frac{p}{\mu_e - \mu_2} + \frac{q}{\mu_e - \mu_1} = \frac{6(\kappa_e + 2\mu_e)}{5\mu_e(3\kappa_e + 4\mu_e)} \quad (11)$$

for κ_e, μ_e . In the case where one of the phases is perfectly soft or rigid the results exhibit a percolation threshold of $p = \frac{1}{2}$. The formula is also symmetric to phase interchange [$\kappa_e(k_1, g_1, k_2, g_2, p) = \kappa_e(k_2, g_2, k_1, g_1, 1 - p)$ etc.]. These facts limit the applicability of the SCM, since most composites have lower percolation thresholds and many are not symmetric [19]. A more realistic formula is obtained using a generalized SCM (GSCM) [13] for the case of a particle of phase 1 surrounded by a spherical shell of phase (embedded in a medium of the effective moduli). The result is complicated [12] and not reproduced here. The GSCM has zero percolation threshold, and is not symmetric under phase interchange. For non-particulate media it is not clear which phase should be associated with the inclusions and which with the matrix. Below we consider both cases. Christensen [12] found that the GSCM provided a better prediction of composite properties than other common methods, so we shall not consider these here. It should also be noted that the volume fraction is the only microstructural information included in the SCM and GSCM results. This means that these formulae are insensitive to the distribution of each phase, or rather that each formula has a “built-in” microstructure, which may or may not match the experimental one.

The difficulty in deriving general theoretical results for predicting the elastic properties of random composites has provided the impetus for the development of rigorous bounds [41]. For orientationally isotropic materials the bounds take the general form [31],

$$\left(\langle \kappa^{-1} \rangle - \frac{4pq(\kappa_2^{-1} - \kappa_1^{-1})^2}{4\langle \tilde{\kappa}^{-1} \rangle + 3\Gamma} \right)^{-1} \leq \kappa_e \leq \langle \kappa \rangle - \frac{3pq(\kappa_2 - \kappa_1)^2}{3\langle \tilde{\kappa} \rangle + 4\Lambda} \quad (12)$$

$$\left(\langle \mu^{-1} \rangle - \frac{pq(\mu_2^{-1} - \mu_1^{-1})^2}{\langle \tilde{\mu}^{-1} \rangle + 6\Xi} \right)^{-1} \leq \mu_e \leq \langle \mu \rangle - \frac{6pq(\mu_2 - \mu_1)^2}{6\langle \tilde{\mu} \rangle + \Theta} \quad (13)$$

where for a variable b , $\langle b \rangle \equiv pb_1 + qb_2$ and $\langle \tilde{b} \rangle \equiv qb_1 + pb_2$. The additional parameters Γ, Λ, Ξ and Θ depend on the level of microstructural information available. If any of the moduli (κ_i or μ_i) are zero then the lower bounds vanishes. Similarly if any of the moduli are infinite the upper bound diverges.

If only the volume fractions of the composite are known

$$\Gamma = \mu_1^{-1}, \quad \Lambda = \mu_2, \quad \Xi = \frac{\kappa_1 + 2\mu_1}{\mu_1(9\kappa_1 + 8\mu_1)} \quad \& \quad \Theta = \frac{\mu_2(9\kappa_2 + 8\mu_2)}{\kappa_2 + 2\mu_2}, \quad (14)$$

and Eqns. (12) & (13) are the bounds of Hashin and Shtrikman [20] for the case $\mu_2 \geq \mu_1$ and $\kappa_2 \geq \kappa_1$. The bounds only apply to well-ordered materials [$(\kappa_2 - \kappa_1)(\mu_2 - \mu_1) \geq 0$] and the inequality signs in the bounds must be reversed if $\mu_2 < \mu_1$ and $\kappa_2 < \kappa_1$. If further information is available in the form of three-point statistical correlations it is possible to derive more restrictive bounds in terms of the microstructure parameters [27],

$$\zeta_1 = \frac{9}{2pq} \int_0^\infty \frac{dr}{r} \int_0^\infty \frac{ds}{s} \int_{-1}^1 du P_2(u) \left(p^{(3)}(r, s, t) - \frac{p^{(2)}(r)p^{(2)}(s)}{p} \right) \quad (15)$$

$$\eta_1 = \frac{5}{21}\zeta_1 + \frac{150}{7pq} \int_0^\infty \frac{dr}{r} \int_0^\infty \frac{ds}{s} \int_{-1}^1 du P_4(u) \left(p^{(3)}(r, s, t) - \frac{p^{(2)}(r)p^{(2)}(s)}{p} \right). \quad (16)$$

where $t^2 = r^2 + s^2 - 2rsu$ and $P_2(u) = \frac{1}{2}(3u^2 - 1)$ and $P_4(u) = \frac{1}{8}(35u^4 - 30u^2 + 3)$ are Legendre polynomials. In this case we have

$$\begin{aligned}\Gamma &= \langle \mu^{-1} \rangle_\zeta, \quad \Lambda = \langle \mu \rangle_\zeta, \quad \Theta = \frac{3\langle \mu \rangle_\eta \langle 6\kappa + 7\mu \rangle_\zeta - 5\langle \mu \rangle_\zeta^2}{\langle 2\kappa - \mu \rangle_\zeta + 5\langle \mu \rangle_\eta} \\ \Xi &= \frac{5\langle \mu^{-1} \rangle_\zeta \langle 6\kappa^{-1} - \mu^{-1} \rangle_\zeta + \langle \mu^{-1} \rangle_\eta \langle 2\kappa^{-1} + 21\mu^{-1} \rangle_\zeta}{\langle 128\kappa^{-1} + 99\mu^{-1} \rangle_\zeta + 45\langle \mu^{-1} \rangle_\eta}.\end{aligned}\quad (17)$$

Here we have used the standard notation $\langle b \rangle_\zeta \equiv \zeta_1 b_1 + \zeta_2 b_2$ and $\langle b \rangle_\eta \equiv \eta_1 b_1 + \eta_2 b_2$ where b_i is any function of μ_i and κ_i , $\zeta_2 = 1 - \zeta_1$ and $\eta_2 = 1 - \eta_1$. With the parameters given in Eqn. (17), the bounds on κ are due to Beran and Molyneux [5] while the bounds on μ are those of Milton and Phan-Thien [28]. The development of these bounds have been recently reviewed [41, 31]. Below we consider the Young's modulus [$E = 9\kappa\mu/(3\kappa + \mu)$] and Poisson's ratio [$\nu = (3\kappa - 2\mu)/(6\kappa + 2\mu)$] of a composite. The bounds on E [19] and ν [50] are

$$\frac{9\kappa_l\mu_l}{3\kappa_l + \mu_l} \leq E_e \leq \frac{9\kappa_u\mu_u}{3\kappa_u + \mu_u} \quad \& \quad \frac{3\kappa_l - 2\mu_u}{6\kappa_l + 2\mu_u} \leq \nu_e \leq \frac{3\kappa_u - 2\mu_l}{6\kappa_u + 2\mu_l}, \quad (18)$$

where the subscripts refer to the upper and lower bound of Eqns. (12) & (13). Depending on the level of microstructural information employed to find the bounds on κ and μ we refer to Eqn. (18) as the Hashin and Shtrikman (HS) or Beran, Molyneux, Milton and Phan-Thien (BMMP) bounds respectively. The microstructure parameters ζ and η have been evaluated for hard and overlapping spheres [41], level cut Gaussian random-field models [37] and can be evaluated for other Boolean models [23].

4.2 Computation

A microstructure made up of a digital image is already naturally discretized and so lends itself to numerical computation of many quantities. For computing elastic moduli, there are two methods available: a finite element method [18], and a finite difference method [29]. The finite element method uses a variational formulation of the linear elastic equations, and finds the solution by minimizing the elastic energy via a fast conjugate gradient method. The finite difference method formulates the linear elastic equations directly in a finite difference approach, and solves the resulting set of linear equations with a similar conjugate gradient method.

For a porous material, with one solid phase and one pore phase, either method can be used, as the zero normal force boundary condition at a solid-pore boundary is easy to handle in either method. When there are solid-solid boundaries between two different phases, the boundary conditions become continuity of displacement and continuity of normal force. This is harder to implement in the finite difference method, while it is just as easy to do as in the solid-pore case for the finite element method. We have used the finite element method exclusively in this paper.

The finite element method is one that has been especially adapted for digital images. It is for linear elasticity only. Each pixel, in 3-D, is taken to be a tri-linear finite element [14]. There can be any number of phases, whether isotropic or anisotropic, as long as each phase can be adequately depicted within the resolution of the digital image used, and can be described with a single elastic moduli tensor. Thermal strains can also be easily handled [17]. The digital image is assumed to have periodic boundary conditions. A strain is applied, with the average stress or the average elastic energy giving the effective elastic moduli [41, 19]. Details of the theory and programs used are reported in the papers of Garboczi & Day [18] and Garboczi [17]. The actual programs are available at <http://ciks.cbt.nist.gov/garboczi/>, Chapter 2.

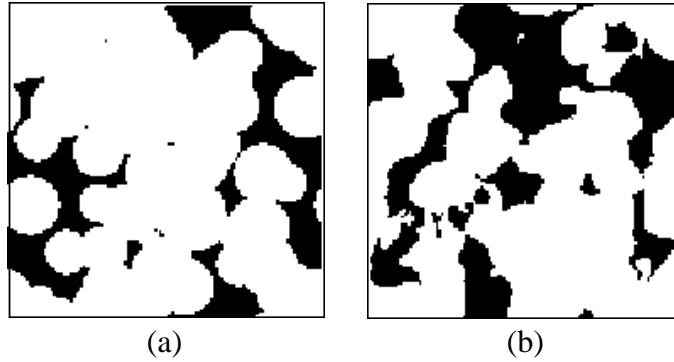


Figure 2: Cross-sections of (a) the overlapping sphere model, and (b) the best reconstruction (model I_{10} $c=0$). The volume fraction is $p=20\%$ and the images are 96×96 pixels.

4.3 Test case: Overlapping sphere model

Before going ahead and reconstructing the W–Ag composite we first tested the procedure for the over-lapping sphere model for which the statistical properties can be analytically evaluated [44]. A 3-D realization of this model is also easy to generate, so that the reconstruction can be carefully tested. The overlapping sphere model [Fig 2(a)] has previously been reconstructed using the models derived from the level cut GRF's [34]. Model I_{10} ($c=0$) was found to be the best reconstruction [Fig 2(b)]. To gauge the accuracy of the procedure for the elastic properties of the tungsten-silver composite (see the following section) we have computed the elastic moduli of the overlapping sphere model and its reconstruction at volume fraction $p = 20\%$ (of the phase outside the spheres). The moduli of each phase at each temperature is set to the corresponding value for silver and tungsten. The results, shown in Fig. 3, indicate that the procedure performs very well. When the silver has non-zero elastic moduli, for temperatures below the melting point of silver, the reconstruction provides an extremely good prediction of E (error $< 1\%$). At temperatures above the melting point of silver, the silver is taken to have zero shear and bulk moduli, and the reconstructed model is 9% stiffer than overlapping spheres. Since the moduli depend most strongly on microstructure at high contrast (contrast = the ratio of the Young's moduli between the two phases) the latter error is likely to be more indicative of the ability of the model to reproduce the microstructure of overlapping spheres. Nevertheless the reconstruction provides a reasonable model. Similar agreement was seen for the Poisson ratios (not shown).

An advantage of the method is that the BMMP bounds [Eqn. (18)] can be evaluated (since $p_{\text{rec}}^{(3)}$ can be computed). The microstructure parameters for the reconstruction [model I_{10} ($c=0$)] were estimated as $\zeta_1 = 0.43$, $\eta_1 = 0.35$ [34]. The bounds (see Fig. 3) are significantly more restrictive than those of Hashin and Shtrikman, and are seen to bound the finite element moduli of both the overlapping sphere and reconstructed models. Above the melting point the lower bounds are identically zero, as we have taken the elastic properties of silver to be zero at this point. Actually, above the melting point of silver, it would be more reasonable to suppose that the silver has a non-zero bulk modulus, with a zero shear modulus. This is only important when comparing with experimental results, however, and not in this model-model comparison.

5 Application to a tungsten-silver composite

To quantitatively test the reconstruction method, experimental data need to be available giving a picture of the material, properties for each individual phase, and overall composite

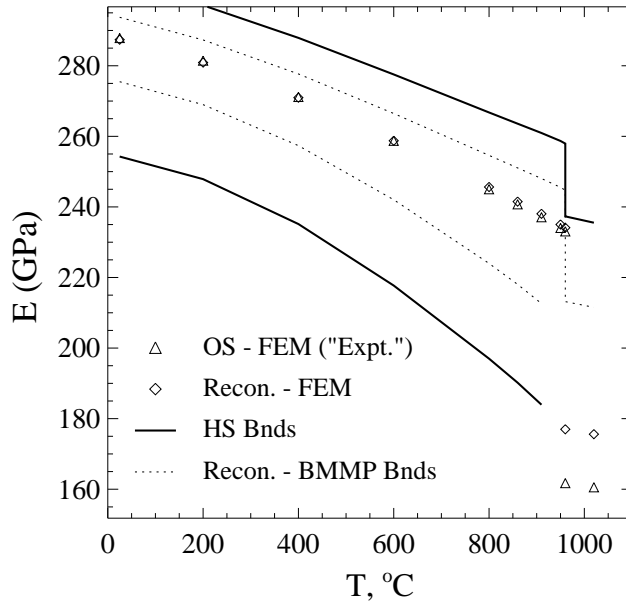


Figure 3: Young’s modulus of the overlapping sphere model (OS) compared with data obtained from the best reconstruction (Recon.) [model I_{10} ($c=0$)] (Finite element method). The Beran, Molyneux, Milton and Phan–Thien (BMMP) bounds are seen to be more restrictive than the Hashin and Shtrikman (HS) bounds for both models.

properties. A well characterized system, suitable to test the reconstruction procedures, is provided by the tungsten-silver (W–Ag) composite of Umekawa *et al.* [45]. This composite was produced by infiltrating a porous tungsten solid with molten silver (volume fraction of silver $p=20\%$). The Young’s modulus of the composite was measured at a range of temperatures above and below the melting point of silver (960°C). The elastic moduli of each phase were obtained by measuring the moduli of pure samples of tungsten and silver at each temperature. This data cannot be used directly because both phases of the composite actually contained tiny spherical pores. These will reduce the Young’s moduli and Poisson’s ratio of each phase. This effect can be accounted for by applying well known results for dilute spherical inclusions [12]. For porous materials (porosity $\phi \ll 1$) the formulae can be rewritten as

$$E_\phi = E_m - \phi E_m \left(\frac{9 - 4\nu_m - 5\nu_m^2}{7 - 5\nu_m} \right) \quad (19)$$

$$\nu_\phi = \nu_m - \frac{3}{2}\phi \left(\frac{(5\nu_m - 1)(1 - \nu_m^2)}{7 - 5\nu_m} \right) \quad (20)$$

where E_m , ν_m denote matrix properties and E_ϕ , ν_ϕ are the porosity modified values. The tungsten matrix had an internal porosity of 1% while the silver phase had a porosity of 10% at room temperature, decreasing linearly to 5% at the melting point. Table 3 shows the phase moduli used at different temperatures.

To reconstruct the W-Ag composite we digitize a photograph of the sample (Fig. 4). All points below a selected threshold grey-level are set to black (the silver phase) while the remainder is set to white. The image was blurred and re-thresholded to remove the pores of the tungsten matrix (which appeared as silver). This had little effect on p_{expt} and $p_{\text{expt}}^{(2)}$, but a significant effect on the measured silver chord distribution. The resulting image is shown in Fig. 5. The image actually has a silver content of only 13.5%, significantly lower than the nominal value of 20%. The statistical properties of the image are compared with those of

Table 3: The moduli of the silver and tungsten phases, as a function of temperature, after being corrected for the internal porosity of each phase.

Temp($^{\circ}$ C)	Silver		Tungsten	
	E(GPa)	ν	E(GPa)	ν
25	71	0.36	400	0.28
200	69	0.36	392	0.28
400	63	0.36	383	0.28
600	54	0.36	373	0.28
800	45	0.37	363	0.28
860	42	0.37	361	0.28
910	39	0.37	359	0.28
950	37	0.37	357	0.28
960	37	0.37	356	0.28
960	0	0.50	356	0.28
1020	0	0.50	354	0.28



Figure 4: The original scanned image from Umekawa *et al.* [45] ($236 \times 204 \mu\text{m}$ at 759×657 pixels). The dark phase corresponds to tungsten and the lighter to silver.

11 trial reconstructions in Table 4, while 2-D slices of the models themselves are shown, for purposes of illustration, in Fig. 6. Several of the models were unable to reproduce $p_{\text{expt}}^{(2)}$ and were considered no further. A comparison of the chord distributions indicated that model N ($c=0$) provided the best reconstruction. The auto-correlation function of this model is compared with experimental data in Fig. 7. The experimental and model chord-distributions are shown in Fig. 8. The silver distribution $\rho_{\text{expt}}^{(1)}$ is well reproduced by the model at all lengths shown, while $\rho_{\text{mod}}^{(2)}$ performs less well at small chord lengths. Two and three dimensional images of the model are shown in Fig. 9 (shown at the same scale as Fig. 5) and in Fig. 10.

For the purposes of computing the elastic properties of the model we maintain the length scale parameters (ξ , r_c and d) and alter the level cut parameters (α and β) of the model such that $p_{\text{rec}}=20\%$ (in accord with the experimental composite). The Young's modulus, computed

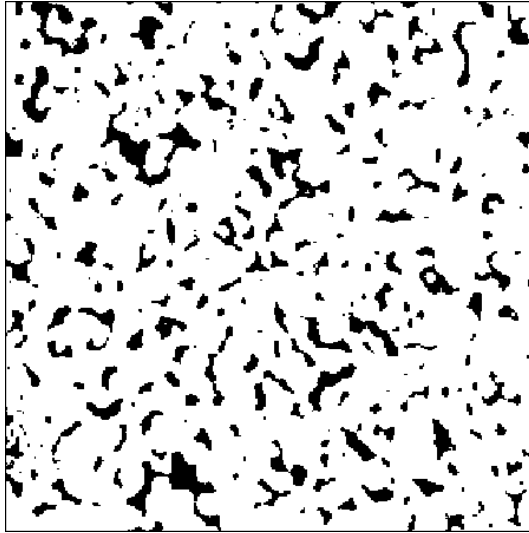


Figure 5: The cropped (640×640 pixels) binary image obtained from the scanned image. This is the sample used to calculate the statistics of the composite (side length $198.7 \mu\text{m}$). The black phase corresponds to silver.

Table 4: A comparison of the statistical properties of 11 reconstructions with those of the experimental composite; $p=13.5\%$ and $s_v=0.17 \mu\text{m}^{-1}$ (obtained from Fig. 5). Many of the models are able to reproduce the low order statistical properties of the composite ($Ep^{(2)} < 0.1$). This shows that $p^{(2)}(r)$ does not uniquely specify composite microstructure.

Mod.	c	r_c	ξ	d	s_v	$Ep^{(2)}$	$E\rho^{(1)}$	$E\rho^{(2)}$
N	0	2.16	2.15	13.0	0.19	0.05	0.03	0.28
N	$\frac{1}{2}$	28.1	28.2	22.0	0.18	0.11		
N	1	∞	∞	25.6	0.18	0.10		
I	0	2.88	2.89	12.5	0.20	0.05	0.28	0.88
I	$\frac{1}{2}$	13.4	13.5	15.9	0.18	0.06	0.32	0.53
I	1	32.7	32.1	17.4	0.17	0.05	0.11	0.38
U	0	2.69	2.68	13.1	0.18	0.05	0.08	0.30
U	$\frac{1}{2}$	60.2	144	35.5	0.20	0.15		
U	1	∞	∞	43.0	0.20	0.15		
I ₁₀	0	4.75	4.76	12.6	0.21	0.06	0.33	0.58
OS		$r_0=3.75$			0.21	0.25	0.49	0.45

using the finite element method, is compared with the experimental data of Umekawa *et al.* in Fig. 11. For the temperature region below the melting point of silver the maximum error is 4%, a very good result. Above the melting point of silver, when the silver phase is taken to have a zero bulk and shear modulus, the error is only 3%. The agreement may actually be better than that, however. Since the elastic measurements were dynamic measurements, the liquid silver can be considered as being trapped on the time scale of the experimental measurement, before any significant flow could take place, and so could still contribute to the effective moduli via its non-zero liquid bulk modulus. Just before melting, the silver had a bulk modulus of about 35GPa. If we take the bulk modulus to be somewhat lower, in analogy

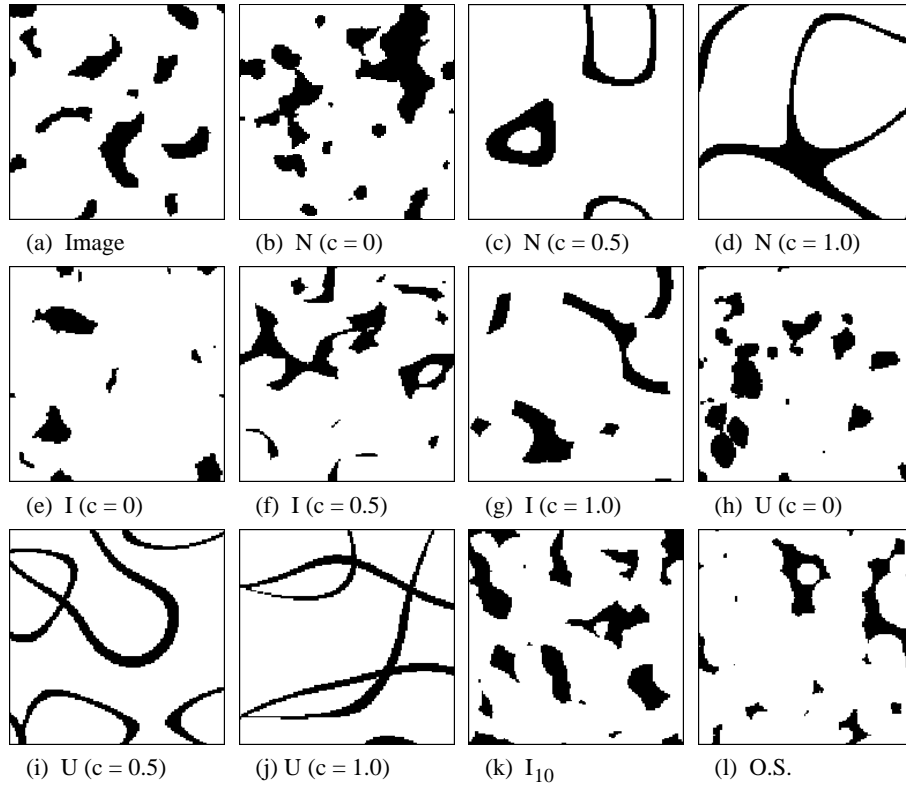


Figure 6: Cross-sections of a portion of the original image (a) and the eleven trial reconstructions (b-l) at $p=13.5\%$. The length-scale parameters of the trials are chosen to match $p_{\text{expt}}^{(2)}(r)$. The chord-distribution's (Table 4) indicate that model N ($c=0$) [shown in (b)] provides the best reconstruction. Each image has side length $39.7\mu\text{m}$.

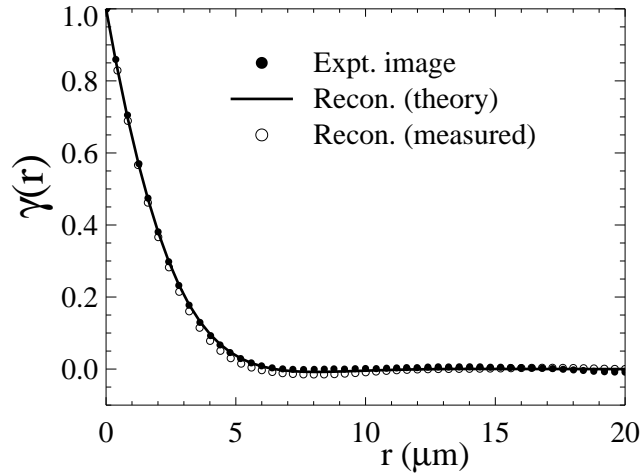


Figure 7: The auto-correlation function of the experimental image is well reproduced by the best reconstruction [model N ($c=0$)].

to the ice-water difference around 0°C , then a bulk modulus of 23.1GPa causes the N ($c=0$) model to agree perfectly with experiment at temperature points above the melting point of silver.

The bounds are also shown in Fig. 11. For model N ($c=0$) the microstructure parameters are $\zeta_1 = 0.31$ and $\eta_1 = 0.27$. The results bound the experimental data and provide a reasonable

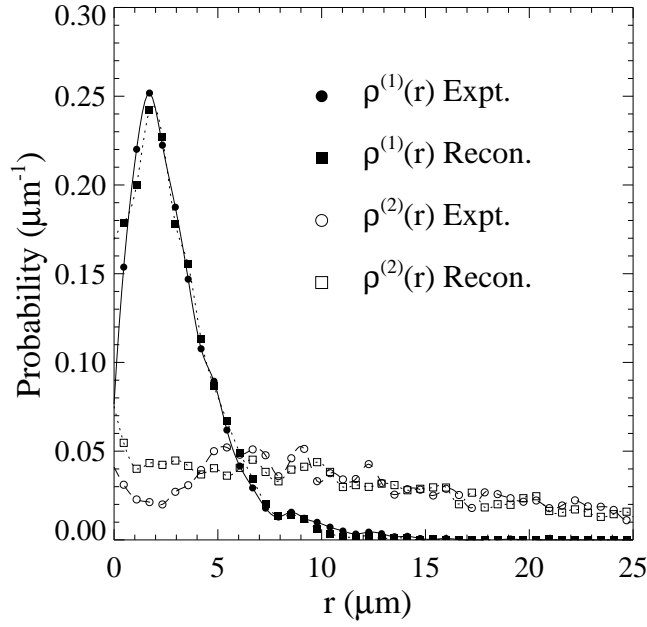


Figure 8: The good agreement between the model and experimental chord distributions [silver: $\rho^{(1)}(r)$; tungsten: $\rho^{(2)}(r)$] indicates that model N ($c=0$) provides the best reconstruction.

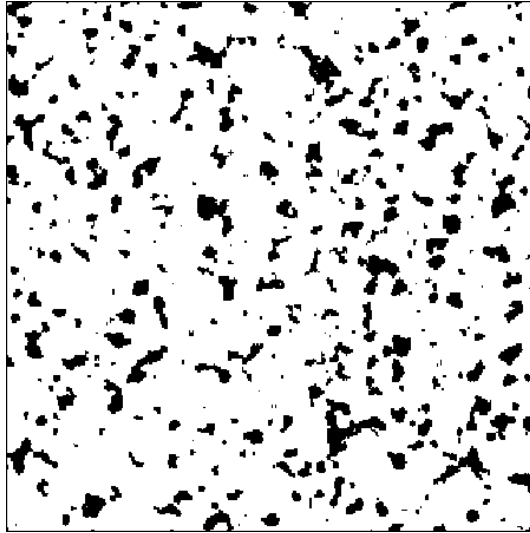


Figure 9: The best reconstruction [model N ($c=0$)]. The region shown is $198.7 \times 198.7 \mu\text{m}$ (cf. Fig. 5).

prediction of the Young's modulus below the melting point of silver. Note that even if the silver phase is given a non-zero bulk modulus past its melting point, the zero shear modulus causes the lower bounds for shear modulus and therefore Young's modulus to be identically zero. Unfortunately, there was no reported Poisson's ratio results for the composite, so we cannot compare to the model results for this quantity.

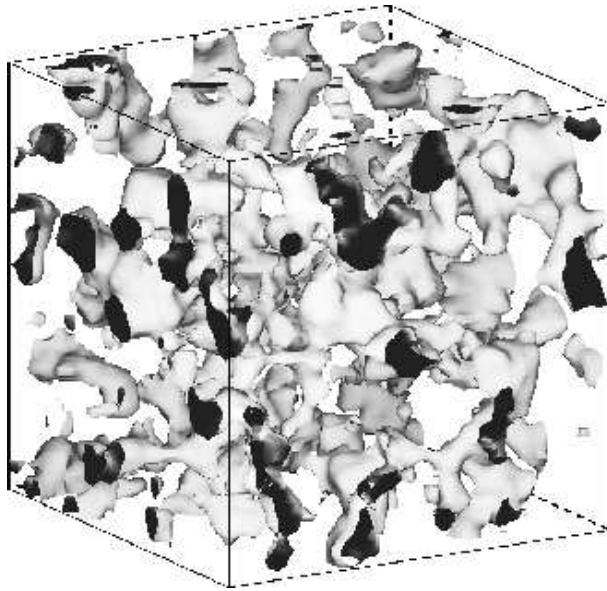


Figure 10: The silver phase (shown as solid) of the best reconstruction [model N ($c=0$)]. The side length is $39.7\mu\text{m}$.

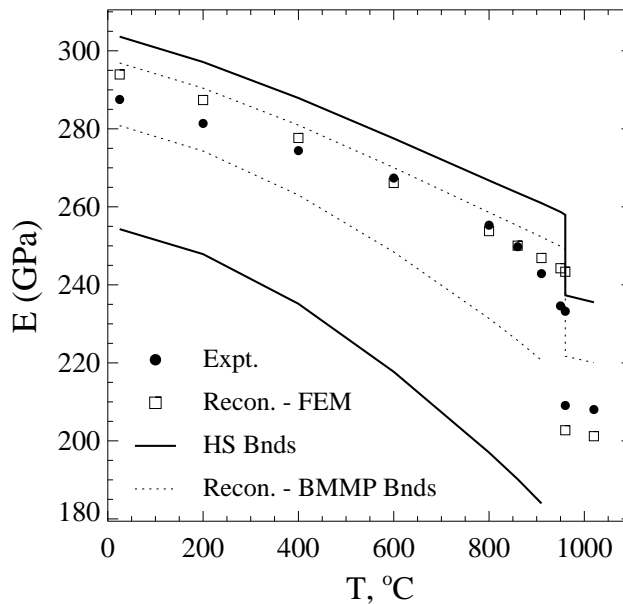


Figure 11: The experimental Young's moduli compared with FEM data obtained from the best reconstruction [Fig. 10]. The Beran, Molyneux, Milton and Phan-Thien (BMMP) bounds for the reconstruction and Hashin and Shtrikman bounds are also shown.

6 Analysis of analytical effective elastic moduli predictions

We now compare the different analytical predictions of effective moduli with the finite element data. We have chosen to study the two most common models and only consider the moduli appropriate for the W-Ag composite studied above. The results are shown in Fig. 12(a) for overlapping spheres and in Fig. 12(b) for the single level-cut GRF or excursion set of Quiblier [model N($c=0$)]. The self-consistent method provides a very good estimate of E_e for model N($c=0$), but not for overlapping spheres. This might be expected because the N($c=0$) model

is symmetric with respect to phase-interchange (like the SCM) while the overlapping sphere model is not. As stated above the application of the generalized SCM is difficult because it is not obvious which phase should be chosen as the ‘inclusion’ phase. For the overlapping sphere model the tungsten phase is comprised of spheres (at 80% volume fraction), so is the more likely choice for the inclusion phase. Nevertheless, we report both estimates (80% W inclusions and 20% Ag matrix or 20% Ag inclusions and 80% W matrix) for both models. For either choice, the GSCM fails to provide an accurate estimate. Indeed, above the melting point of silver the GSCM vanishes for the case 20% Ag matrix case since the matrix phase is now completely soft. For the overlapping sphere model the Beran, Molyneux, Milton and Phan–Thien bounds are calculated using the microstructure parameters $\zeta_1 = 0.52$, $\eta_1 = 0.42$ [44, 9]. Below the melting point of silver (where the contrast between the phases is moderate) the upper bounds provide a very good estimate of the effective moduli.

A brief discussion of the effect of elastic contrast is necessary here. We have already noted that the analytical predictions of effective moduli do not explicitly depend on microstructure, but have a “built-in” microstructure. The elastic contrast, the ratio between the phase moduli, will determine how sensitive the effective moduli actually are to microstructure. For example, in the case of a two-phase composite having equal shear moduli but different bulk moduli, there is a simple exact formula for the effective bulk modulus which is totally insensitive to microstructure [21]. In the case of small contrast, the effective moduli can be expressed exactly as a power series in the moduli differences [42]. Up to second order in this difference, at any volume fraction, the coefficients of the power series are not dependent on anything but the volume fractions and the individual phase properties. Therefore at small contrast, analytical predictions of effective moduli that explicitly depend only on volume fractions and phase moduli should all work well.

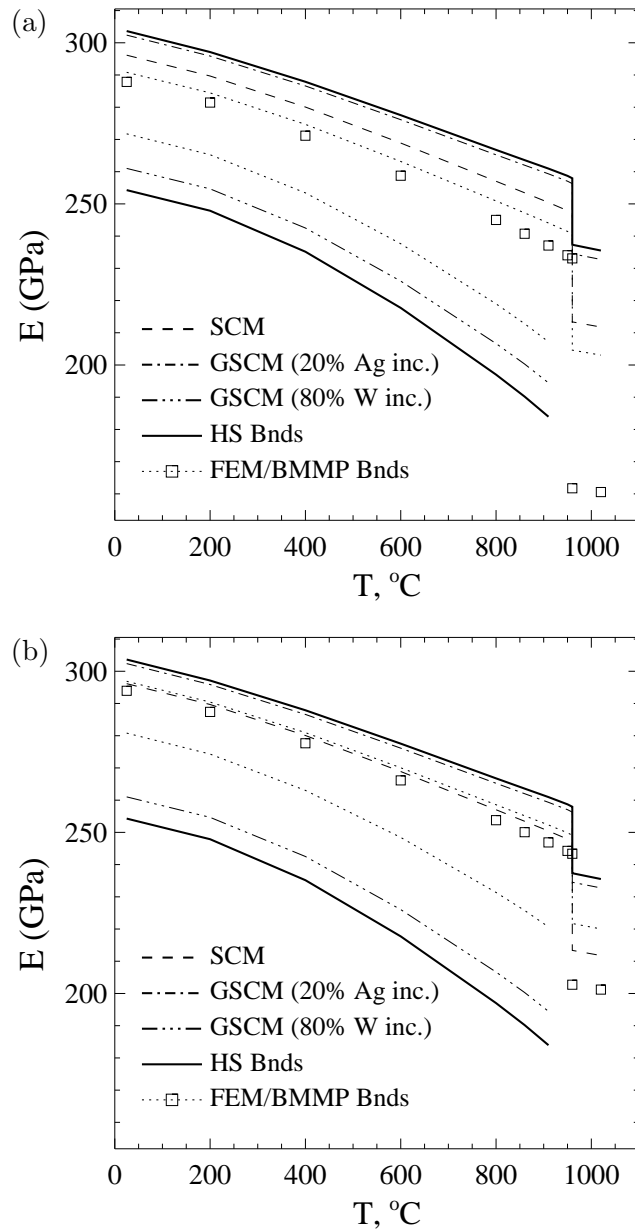


Figure 12: Comparison of theory (predictions and bounds) with finite element (FEM) calculations for the Young's modulus of (a) the overlapping sphere model and (b) the single-cut GRF model [$N(c=0)$, see Fig. 10]. The standard (SCM) and generalized (GSCM) self-consistent methods are shown, as are the Hashin and Shtrikman (HS) and Beran, Molyneux, Milton, and Phan–Thien (BMMP) bounds.

7 Conclusion

Throughout this paper, we have treated the finite element computation method as being perfectly accurate, so that comparisons of elastic results to experiment were solely a test of how well the reconstructed microstructure compared to the real microstructure. This is not exactly true, since there are numerical errors in the finite element method [18, 17]. These are small, however, and are generally of about the same size or less than the differences seen between model computations and experimental data for the elastic moduli. There are also statistical sampling errors associated with the finite size ($\approx 40\mu\text{m}$) of the models we employ to estimate the elastic properties. Since this is much greater than the correlation length of the samples ($\approx 5\mu\text{m}$ - see Fig. 7) we again assume these errors to be small. Therefore, the good agreement between model prediction and experimental data seen in this paper is good evidence that the model considered is indeed capturing the main aspects of the experimental microstructure.

We have compared various theoretical results to finite element computations of the effective Young's modulus E_e for non-particulate media: a W-Ag composite and two model media (overlapping spheres and a single-cut Gaussian random field). The generalized self-consistent method (derived for particulate composites) did not provide a good estimate of E_e for the bi-continuous materials considered here. The standard self-consistent method provided a good estimate for the single-cut GRF and W-Ag composite. Since the method predicts zero moduli for porosity above 50% but the solid phase of the single-cut GRF remains connected up to porosities of around 90% [37] such agreement cannot be general. Upper bounds, calculated using three-point statistical correlation functions, provided a good prediction at low contrast ($E_1/E_2 \approx 6$) for each composite. When one of the phases was completely soft the bounds lost predictive value. Therefore, for general composites, it is important to employ numerical computations of the effective moduli. For accurate numerical prediction of composite properties it is important that a realistic model be used. Model-based statistical reconstruction, based on the Joshi-Quiblier-Adler approach, appears to be a viable route for microstructural simulation. However, it is important that the models underlying the procedure be capable of mimicking the composite microstructure. We have shown how several different models can be employed to find a useful reconstruction.

ACKNOWLEDGMENTS

A.R. thanks the Australian-American Educational Foundation (Fulbright Commission) for financial support and the Department of Civil Engineering and Operations Research at Princeton University where this work was completed. We also thank the Partnership for High-Performance Concrete program of the National Institute of Standards and Technology for partial support of this work.

References

- [1] ADLER, P. M. *Porous Media*. Butterworth-Heinemann, Boston, 1992.
- [2] ADLER, P. M., JACQUIN, C. G., AND QUIBLIER, J. A. Flow in simulated porous media. *Int. J. Multiphase Flow* 16 (1990), 691–712.
- [3] ADLER, P. M., JACQUIN, C. G., AND THOVERT, J.-F. The formation factor of reconstructed porous media. *Water Resources Res.* 28 (1992), 1571–1576.
- [4] BENTZ, D. P., AND MARTYS, N. S. Hydraulic radius and transport in reconstructed model three-dimensional porous media. *Trans. Porous Media* 17 (1994), 221–238.

- [5] BERAN, M., AND MOLYNEUX, J. Use of classical variational principles to determine bounds for the effective bulk modulus in heterogeneous media. *Q. Appl. Math.* 24 (1966), 107–118.
- [6] BERGMAN, D. J. The dielectric constant of a composite material—a problem in classical physics. *Phys. Repts.* 43 (1978), 377–407.
- [7] BERK, N. F. Scattering properties of a model bicontinuous structure with a well defined length scale. *Phys. Rev. Lett.* 58 (1987), 2718–2721.
- [8] BERRYMAN, J. G. Measurement of spatial correlation functions using image processing techniques. *J. Appl. Phys.* 57 (1985), 2374–2384.
- [9] BERRYMAN, J. G. Variational bounds on elastic constants for the penetrable sphere model. *J. Phys. D* 18 (1985), 585–597.
- [10] BOURGEOIS, F. S., AND LYMAN, G. J. Morphological analysis and modelling of fine coal filter cake microstructure. *Chem. Eng. Sci.* 52 (1997), 1151–1162.
- [11] BUDIANSKY, B. On the elastic moduli of some heterogeneous materials. *J. Mech. Phys. Solids* 13 (1965), 223–227.
- [12] CHRISTENSEN, R. M. A critical evaluation for a class of micro-mechanics models. *J. Mech. Phys. Solids* 38 (1990), 379–404.
- [13] CHRISTENSEN, R. M., AND LO, K. H. Solutions for effective shear properties in three phase sphere and cylinder models. *J. Mech. Phys. Solids* 27 (1979), 315–330.
- [14] COOK, R., MALKUS, D., AND PLESHA, M. *Concepts and Applications of Finite Element Analysis*. J. Wiley and Sons, New York, 1989.
- [15] CROSSLEY, P. A., SCHWARTZ, L. M., AND BANAVAR, J. R. Image-based models of porous-media - application to vycor glass and carbonate rocks. *Appl. Phys. Lett.* 59 (1991), 3553–3555.
- [16] FLANNERY, B. P., DECKMAN, H. W., ROBERTS, W. G., AND DAMICO, K. L. 3-dimensional x-ray microtomography. *Science* 237 (1987), 1439.
- [17] GARBOCZI, E. J., 1998. NIST Internal Report 6269, available at <http://ciks.cbt.nist.gov/garbocki/>, Chapter 2.
- [18] GARBOCZI, E. J., AND DAY, A. R. An algorithm for computing the effective linear elastic properties of heterogeneous materials: Three-dimensional results for composites with equal phase poisson ratios. *J. Mech. Phys. Solids* 43 (1995), 1349–1362.
- [19] HASHIN, Z. Analysis of composite-materials - a survey. *J. Appl. Mech.* 50 (1983), 481–505.
- [20] HASHIN, Z., AND SHTRIKMAN, S. A variational approach to the theory of the elastic behaviour of multiphase materials. *J. Mech. Phys. Solids* 11 (1963), 127–140.
- [21] HILL, R. Elastic properties of reinforced solids: Some theoretical principles. *J. Mech. Phys. Solids* 11 (1963), 357–372.
- [22] HILL, R. A self-consistent mechanics of composite materials. *J. Mech. Phys. Solids* 13 (1965), 213–222.

- [23] JEULIN, D., AND SAVARY, L. Effective complex permittivity of random composites. *J. Physique I* 7 (1997), 1123–1142.
- [24] JOSHI, M. *A class of stochastic models for porous materials*. PhD thesis, Univ. of Kansas, Lawrence, 1974.
- [25] KING, R. P. Random geometrical models for porous media and other two-phase materials. *Chem. Eng. J.* 52 (1996), 1151–1162.
- [26] KWIECIEN, M. J., MACDONALD, I. F., AND DULLIEN, F. A. L. Three-dimensional reconstruction of porous sandstone from serial section data. *J. Micros.* 159 (1990), 343–359.
- [27] MILTON, G. W. Bounds on the electromagnetic, elastic, and other properties of two-component composites. *Phys. Rev. Lett.* 46 (1981), 542–545.
- [28] MILTON, G. W., AND PHAN-THIEN, N. New bounds on effective elastic moduli of two-component materials. *Proc. Roy. Soc. London A* 380 (1982), 305–331.
- [29] POUTET, J., MANZONI, D., HAGE-CHEHADE, F., JACQUIN, C. G., BOUTECA, M. J., THOVERT, J. F., AND ADLER, P. M. The effective mechanical properties of random porous media. *J. Mech. Phys. Solids* 44 (1996), 1587–1620.
- [30] QUIBLIER, J. A. A new three-dimensional modeling technique for studying porous media. *J. Colloid Interface Sci.* 98 (1984), 84–102.
- [31] QUINTANILLA, J. Microstructure and properties of random heterogeneous materials: A review of theoretical results. *Polymer Eng. Sci.* (1998). (To be published).
- [32] RICE, S. O. The mathematical analysis of random noise. *Bell Sys. Tech. J.* 23 (1944), 282–332. **24**, 46–156, 1945.
- [33] ROBERTS, A. P. Morphology and thermal conductivity of model organic aerogels. *Phys. Rev. E* 55 (1997), 1286–1289.
- [34] ROBERTS, A. P. Statistical reconstruction of three-dimensional porous media from two-dimensional images. *Phys. Rev. E* 56 (1997), 3023–3212.
- [35] ROBERTS, A. P., AND KNACKSTEDT, M. A. Mechanical and transport properties of model foamed solids. *J. Mat. Sci. Lett.* 14 (1995), 1357–1359.
- [36] ROBERTS, A. P., AND KNACKSTEDT, M. A. Structure-property correlations in model composite materials. *Phys. Rev. E* 54 (1996), 2313–2328.
- [37] ROBERTS, A. P., AND TEUBNER, M. Transport properties of heterogeneous materials derived from gaussian random fields: Bounds and simulation. *Phys. Rev. E* 51 (1995), 4141–4154.
- [38] SAHIMI, M. Flow, dispersion, and displacement processes in porous media and fractured rocks: From continuum models to fractals, percolation, cellular automata and simulated annealing. *Rev. Mod. Phys.* 65 (1993), 1393–1534.
- [39] STOYAN, D., KENDALL, W. S., AND MECKE, J. *Stochastic geometry and its applications*, 2nd ed. Wiley, Chichester, 1995.
- [40] TEUBNER, M. Level surfaces of gaussian random fields and microemulsions. *Europhys. Lett.* 14 (1991), 403–408.

- [41] TORQUATO, S. Random heterogeneous media: Microstructure and improved bounds on effective properties. *Appl. Mech. Rev.* 44 (1991), 37–76.
- [42] TORQUATO, S. Effective stiffness tensor of composite media-i. exact series expansions. *J. Mech. Phys. Solids* 45 (1997), 1421–1448.
- [43] TORQUATO, S., AND LU, B. Chord-length distribution function for two phase random media. *Phys. Rev. E* 47 (1993), 2950–2953.
- [44] TORQUATO, S., AND STELL, G. Microstructure of two-phase random media. iii. the n-point matrix probability functions for fully penetrable spheres. *J. Chem. Phys.* 79 (1983), 1505–1510.
- [45] UMEKAWA, S., KOTFILA, R., AND SHERBY, O. D. Elastic properties of a tungsten-silver composite above and below the melting point of silver. *J. Mech. Phys. Solids* 13 (1965), 229–235.
- [46] WEISSBERG, H. L. Effective diffusion coefficient in porous media. *J. Appl. Phys.* 34 (1963), 2636–2639.
- [47] WILLIS, J. R. Variational and related methods for the overall properties of composites. *Adv. Appl. Mech.* 21 (1981), 1–78.
- [48] YAO, J., FRYKMAN, P., KALAYDJIAN, F., THOVERT, J.-F., AND ADLER, P. M. High-order moments of the phase function for real and reconstructed model porous media: A comparison. *J. Colloid Interface Sci.* 156 (1993), 478–490.
- [49] YEONG, C. L. Y., AND TORQUATO, S. Reconstructing random media. *Phys. Rev. E* 57 (1998), 495–506.
- [50] ZIMMERMAN, R. W. Hashin-shtrikman bounds on the poisson ratio of a composite material. *Mech. Res. Comm.* 19 (1992), 563–569.